Magnetism and morphology of Co nanocluster superlattices on $GdAu_2$/Au(111)–(13 × 13)

A. Cavallin,[1,*] L. Fernández,[2] M. Ilyn,[3] A. Magaña,[4] M. Ormaza,[2] M. Matena,[2] L. Vitali,[3,5] J. E. Ortega,[2,3,4] C. Grazioli,[6,7] P. Ohresser,[8] S. Rusponi,[1] H. Brune,[1] and F. Schiller[3]

[1]*Institute of Condensed Matter Physics (ICMP), École Polytechnique Fédérale de Lausanne (EPFL), CH-1015 Lausanne, Switzerland*
[2]*Donostia International Physics Center, E-20018 Donostia–San Sebastián, Spain*
[3]*Centro de Física de Materiales (CSIC-UPV-EHU) and Materials Physics Center (MPC), E-20018 Donostia–San Sebastián, Spain*
[4]*Departamento de Física Aplicada I, Universidad del País Vasco, E-20018 Donostia–San Sebastián, Spain*
[5]*Ikerbasque, Basque Foundation for Science, E-48011 Bilbao, Spain*
[6]*Department of Chemical and Pharmaceutical Sciences, University of Trieste, I-34127 Trieste, Italy*
[7]*CNR-IOM, Laboratorio TASC, Basovizza, I-34149 Trieste, Italy*
[8]*Synchrotron SOLEIL, L'Orme des Merisiers, Saint-Aubin, F-91192 Gif-sur-Yvette, France*

(Received 4 February 2014; revised manuscript received 12 November 2014; published 10 December 2014)

We present a comprehensive study of the magnetism and morphology of an ultrahigh density array of Co nanoclusters self-assembled on the single atomic layer $GdAu_2$ on Au(111) template surface. Combining scanning tunneling microscopy, x-ray magnetic circular dichroism, and magneto-optical Kerr effect measurements, we reveal a significant enhancement of the perpendicular magnetic anisotropy energy for noncoalesced single atomic layer nanoclusters compared to Co/Au(111). For coverages well beyond the onset of coalescence, we observe room-temperature in-plane magnetic remanence.

DOI: 10.1103/PhysRevB.90.235419 PACS number(s): 36.40.Cg, 75.75.−c, 81.16.Dn

I. INTRODUCTION

A single atomic layer of $GdAu_2$ forms a moiré pattern on Au(111) with (12 × 12) unit cells of the alloy monolayer adsorbed onto (13 × 13) substrate unit cells. This strain relief pattern is an ideal template for the self-assembly of magnetic nanocluster superlattices [1] as it features a hexagonal array of preferential nucleation sites with the extremely high density of 53 Tera/inch^2 [2,3]. Previous reports of room-temperature magnetic remanence for Co nanoclusters on this surface [4] spurred further investigation on this system, motivated also by the behavior reported for Co nanocluster arrays grown on other templates, such as Au(788) [5], graphene/Ir(111) [6], and hexagonal-BN/Rh(111) [7], which are superparamagnetic down to 40 K or even below. For a nanocluster, the observation of magnetic remanence at a given temperature critically depends on its magnetic anisotropy energy (MAE), which is influenced by the cluster size and shape, as well as by its interaction with the substrate. In this respect, the presence of Gd atoms in contact with Co can significantly influence the MAE because of exchange coupling between Gd 4f and 5d electrons and because of hybridization between Gd 5d and Co 3d orbitals [8]. Moreover, understanding of the directional dependence and magnitude of the MAE of Gd and of Gd compounds represents an active field of research for *ab initio* calculations [9–11].

In this paper we present an in-depth investigation of the growth and magnetism of Co nanoclusters on $GdAu_2$/Au(111). We combine scanning tunneling microscopy (STM), x-ray magnetic circular dichroism (XMCD), and magneto-optical Kerr effect (MOKE) to identify the preferred magnetization direction and the size threshold for magnetic remanence at room temperature and below. We observe magnetic remanence at room temperature only after deposition of more than 3 monolayers (ML; 1 ML is defined as one Co atom per Au(111)-substrate atom [12]). At this coverage the clusters have coalesced and extend over several moiré unit cells. Thus, a combined investigation of the nanocluster morphology and magnetism is mandatory to determine the morphological and magnetic coalescence thresholds, as well as their influence on the onset of remanence at a given temperature.

II. METHODS

Combined STM and MOKE measurements were carried out in two different ultrahigh vacuum chambers at a base pressure of 5×10^{-11} mbar. The first is located in Lausanne and has been designed to perform growth, polar, and transverse MOKE, as well as variable temperature (VT) STM [13] with the sample held at the same position enabling continuous control of its temperature (40–1400 K) and thereby preservation of metastable structures. To achieve a precision of the absolute temperature reading of 1 K, the thermocouple wires were directly attached to the crystal, each of the two wires at separate locations ensuring that the hot junction of the thermoelement is on the crystal [14]. Additional MOKE experiments in longitudinal geometry were performed in the second ultrahigh vacuum chamber equipped with an Omicron VT-STM and located in San Sebastian. The Au(111) substrate was prepared *in situ* by cycles of room temperature Ar^+ ion sputtering at 1 keV followed by annealing to 800 K. The quality of the sample was checked by Auger electron spectroscopy and STM showing the characteristic herringbone pattern of the $(22 \times \sqrt{3})$ surface reconstruction [15,16]. The $GdAu_2$ monolayer was grown by evaporation of Gd from an e-beam heated Mo crucible at a deposition rate of 0.5 ML/min. The influence of the growth temperature and of the Gd coverage on the template quality are discussed below.

Co nanocluster arrays were grown by Co deposition from a carefully outgassed Co rod (purity 99.995% Alfa Aesar) onto

*Present address: Max Planck Institute of Microstructure Physics, D-06120 Halle/Saale, Germany.

the substrate held at room temperature using a commercial *e*-beam evaporator. We have calibrated our source on the clean Au(111) surface by measuring the areal fraction of the surface covered by Co and multiplying it by 2, accounting for the fact that Co forms double layer islands at 300 K [17]. The Co flux was adjusted to 0.14 ML/min.

XMCD measurements at the Co $L_{2,3}$ and Gd $M_{4,5}$ absorption edges were carried out in the total electron yield mode (TEY) at the DEIMOS beamline [18] at Soleil, and at the Circular Polarization (CiPo) beamline [19] at Elettra. In the first case, the magnetic field was applied parallel to the photon beam, in the second, the sample was measured in remanence after application of a 0.5-T field. In both experiments, the samples were measured in normal and grazing incidence. Co coverage (Θ) estimations were obtained by STM at the DEIMOS beamline and at CiPo by comparison with the Co/Au(111) spin-reorientation transition occurring at $\Theta = 4.5$ ML [20,21]. Both calibration methods yield relative coverage uncertainties smaller than $\pm 20\%$. Applications of the XMCD sum rules [22,23] yield the atomic effective spin magnetic moment μ_{S+nD}, where nD is the contribution from the dipole operator, with $n = 7$ for Co and $n = 6$ for Gd, and the orbital magnetic moment μ_L. The values presented in this paper are obtained assuming the bulk values for the number of holes of Co [24] and Gd [25].

III. RESULTS

A. Template quality

The best template homogeneity was obtained at 600-K deposition temperature and subsequent annealing at 700 K for 180 s; see Fig. 1(a). The amount of deposited Gd was precisely adjusted to 0.33 ML to achieve a complete $GdAu_2$ atomic layer, as checked by STM for each newly prepared sample. The $GdAu_2$ alloy formation occurs by insertion of the Gd atoms in the Au(111) surface layer with a simultaneous expansion of the surface layer itself, as suggested by the irregular step shape after the alloy formation in contrast to the clean Au(111) surface that exhibits perfectly straight $\langle 1\bar{1}0\rangle$-oriented steps. The annealing temperature and the Gd coverage are critical parameters for the quality of the template and for the subsequent self-assembly. Annealing below 700 K produces an imperfect moiré pattern, see Fig. 1(b), while deposition of a Gd amount only slightly larger than optimum leads to bilayer-high $GdAu_2$ islands [2], see Fig. 1(c). We found that the growth and magnetism of Co nanoclusters on a compositionally or structurally imperfect $GdAu_2$ layer are very different from the ones on the perfect template. For this reason we paid particular attention to verify the optimal substrate preparation for each of the MOKE and XMCD experiments presented here.

B. Below the coalescence threshold

An ideal $GdAu_2$/Au(111)-(13 × 13) template results in excellent long-range order and homogeneity of the nanocluster arrays as shown for a Co coverage of $\Theta = 0.5$ ML in Fig. 1(d). Figure 1(g) shows a nanocluster area histogram obtained from many STM images taken for each of the indicated coverages. For $\Theta = 0.5$ ML we find a mean area of 500 Å^2 and negligible coalescence since the small peak at around twice the mean

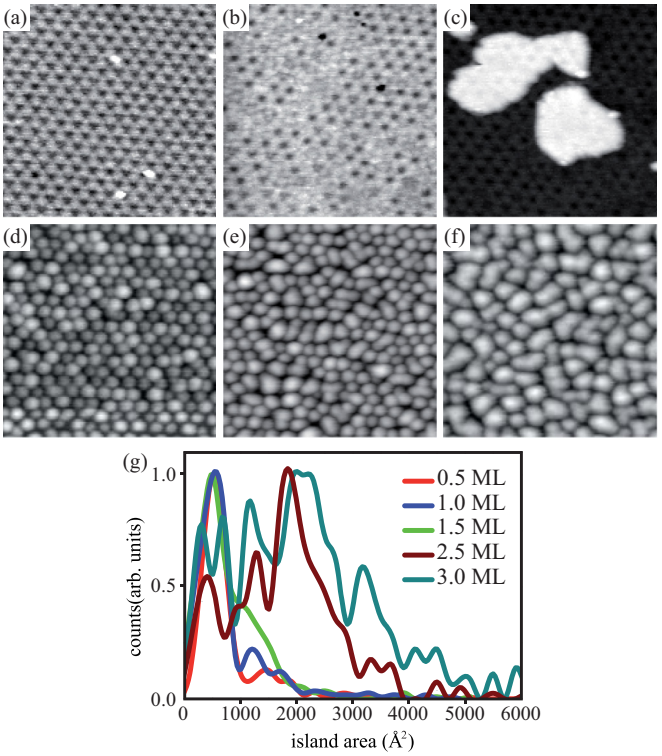

FIG. 1. (Color online) STM images of (a) optimal $GdAu_2$/Au(111) template, see text, (b) imperfect template upon annealing to 600 K only, or by (c) 20% too high Gd coverage. Morphology of Co nanoclusters grown at 300 K on optimally prepared template for increasing coverages of (d) 0.5 ML, (e) 1.5 ML, (f) 3.0 ML. Size of all STM images 50 × 50 nm^2. (g) Histograms of the nanocluster areas.

size is comparable to the noise. The cluster heights are mainly one and two atomic layers (AL) with only a few islands being three atomic layers high. At $\Theta = 1.0$ ML a small shoulder evolves, whose intensity becomes significant at 1.5 ML, which we therefore define as the coalescence onset. The STM image in Fig. 1(e) shows that at this coverage roughly one-third of the clusters have coalesced and occupy two moiré cells. Going to $\Theta = 2.5$ ML, the histogram presents three well defined peaks at approximately 500, 1250, and 1850 Å^2, which we ascribe to clusters extending over one, two, and three superlattice cells, respectively. Clearly, increasing Θ leads to further coalescence. For example, at 3.0 ML a non-negligible fraction of the clusters has areas above 4000 Å^2; see Fig. 1(f). Note that the above areas, directly obtained from STM images, are generally overestimated due to the finite tip radius.

Element specific Co and Gd XMCD recorded for 0.75 ML—where coalescence is negligible—show opposite signs for $|\mu_0 H| < 2$ T, implying an antiferromagnetic alignment of Co and Gd moments; see Fig. 2(a). The acquisition temperature of 30 K is well above the Curie temperature $T_C =$ 19 K of the bare 1-ML $GdAu_2$ substrate deduced from the Arrott plot [26] analysis shown in Fig. 3. Therefore the AFM coupling is a remarkable example of the magnetic proximity effect [27]. At larger fields the Gd signal is dominated by the paramagnetic contribution of Gd atoms which are not exchange-coupled to the Co clusters. The comparison between

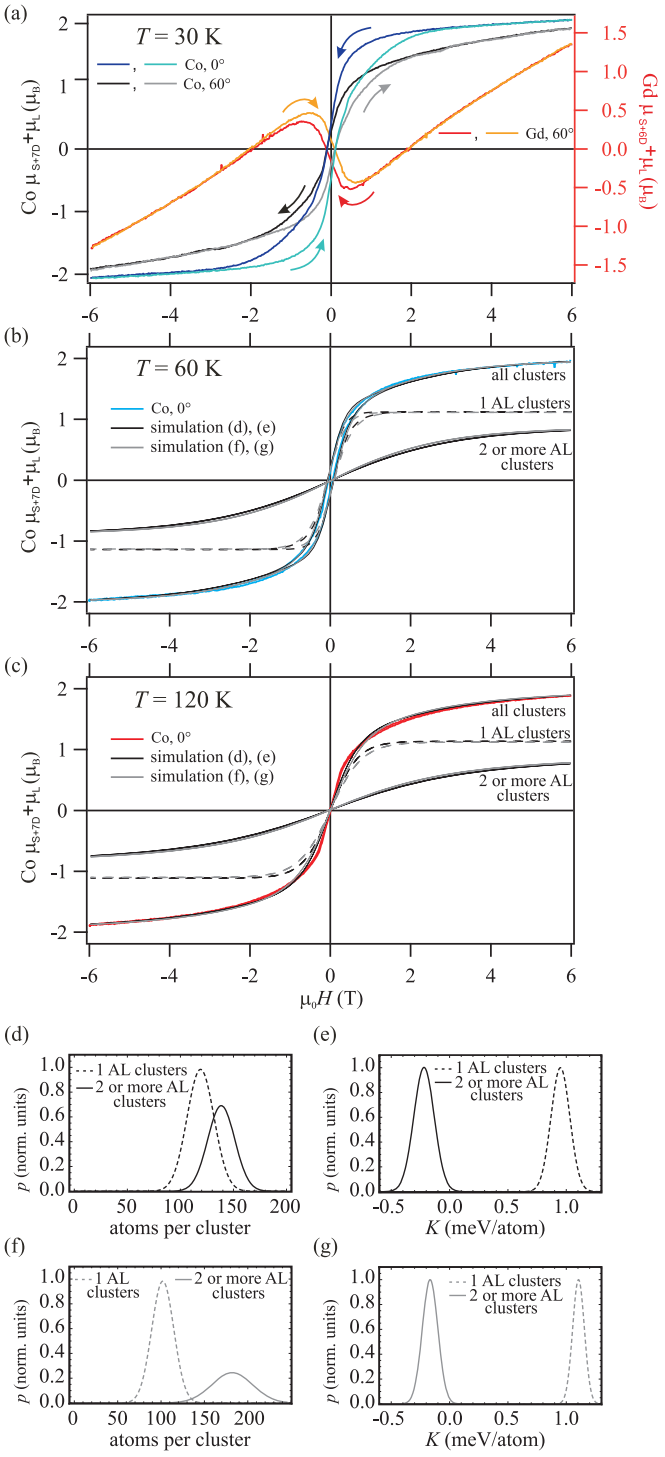

FIG. 2. (Color online) Magnetization curves acquired at the Co L_3 and Gd M_5 edges for normal ($\theta = 0°$) and grazing ($\theta = 60°$) incidence of the photon beam and for $\Theta = 0.75$ ML. XMCD data points close to zero field ($\mu_0|H| < 0.1$ T) have been interpolated because the TEY signal is strongly perturbed there. Experimental magnetization curves at (a) $T = 30$ K, (b) 60 K, and (c) 120 K. For 60 and 120 K the curves are numerically fitted with two sets of size (d),(f) and anisotropy (e),(g) distributions described in the text.

normal and grazing Co magnetization curves at 30 K, together with geometrical information from STM and recent DFT calculations predicting an out-of-plane easy axis for 1-AL-thick clusters and an in-plane easy axis for thicker ones [28], support a mixed configuration with cluster height-dependent easy axes.

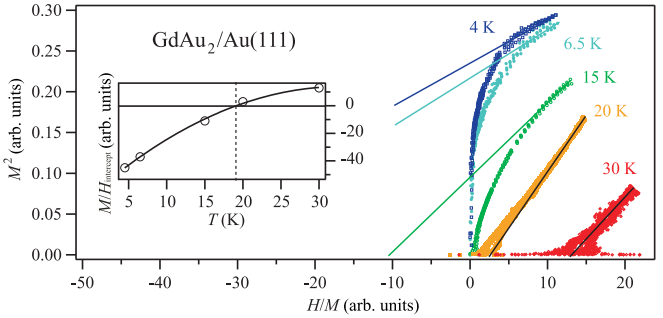

FIG. 3. (Color online) Arrott plot (M^2 vs H/M) of the magnetization of a single atomic layer of $GdAu_2$ on Au(111). The linearly extrapolated high-field data, shown as continuous lines, intercept the origin at the Curie temperature. This occurs at 19 K, as shown in the inset.

In order to quantify the cluster height dependent magnetic anisotropy we numerically fit the magnetization curves at 60 and 120 K, using the method described in Refs. [13,29] for out-of-plane easy axis clusters, and Eq. (3) of Ref. [30] for in-plane easy axis clusters. At these temperatures, the Gd-Co AFM coupling is partly overcome allowing us to neglect the contribution of Gd moments to the Co cluster magnetization dynamics. Following the DFT predictions [28], out-of-plane and in-plane anisotropies are assigned to 1 AL and to thicker clusters, respectively. The cluster magnetization reversal energy barriers are calculated multiplying the magnetic anisotropy energy per atom K (including the shape anisotropy) by the number of atoms per cluster. This is done separately for 1-AL-high and for thicker clusters, whose contributions are then summed. Two size and anisotropy distributions have been considered; see Figs. 2(d) and 2(f). Both size distributions are bimodal and have the same mean size given by the coverage [31]. However, in the first case the two Gaussians representing the size of the 1-AL and of the thicker islands are significantly closer together than in the second case; see Figs. 2(d) and 2(e) vs Figs. 2(f) and 2(g). Both approaches fit the experiment very well and yield similar anisotropy values. The magnetic anisotropy of 1-AL clusters is centered at $+0.95 \pm 0.10$ [$+1.11 \pm 0.06$] meV/atom, and the one of thicker clusters at -0.22 ± 0.10 [-0.17 ± 0.08] meV/atom; see Fig. 2(e) [2(g)]. The fits indicate a fraction of 59% [69%] of all clusters being 1 AL, in good agreement with the morphology observed by STM. The finite widths of the K distributions implies that additional parameters to the size and height determine the anisotropy. Islands with identical size and height can have different shapes of their atomic layers, and for two layer high islands the fraction of atoms in the two layer can be different. Both are expected to have an influence on the overall K of an island.

The perpendicular magnetic anisotropy energy of 1 AL high clusters is considerably larger than the ones reported for 2-AL-high Co islands with comparable size grown on Au(111) and Au(788). The reported values include the shape anisotropy and are $K = 0.25$–0.42 meV/atom [32], 0.3 meV/atom [33] on Au(111), and $K = 0.22 \pm 0.19$ meV/atom [29],

0.37 ± 0.04 meV/atom [5] on Au(788). Therefore the MAE of 1-AL islands on $GdAu_2$/Au(111) is significantly larger than the one of 2-AL Co islands grown on Au(111) and Au(788). The origin of this distinct behavior cannot be attributed to the island shape, which is similar in all these systems, nor to the magnetization reversal mechanism, being coherent rotation for islands smaller than a few nanometers in diameter. Thus, our observations reveal that the Co-Gd coupling substantially increases the thermal stability of the island magnetization.

C. Above the coalescence threshold

We now address the magnetic properties for coverages above the morphological coalescence threshold of 1.5 ML. Figure 4 presents XAS and XMCD spectra recorded at remanence. We note as B_- and B_+ the spectra acquired after exposing the sample to an external magnetic field of 0.5 T, applied in the directions indicated in Fig. 4(a). A remanent in-plane dichroic signal $B_+ - B_-$ is detected at $\Theta = 3.1$ ML and $T = 85$ K. This signal is strongly attenuated when measuring in out-of-plane geometry, as becomes evident

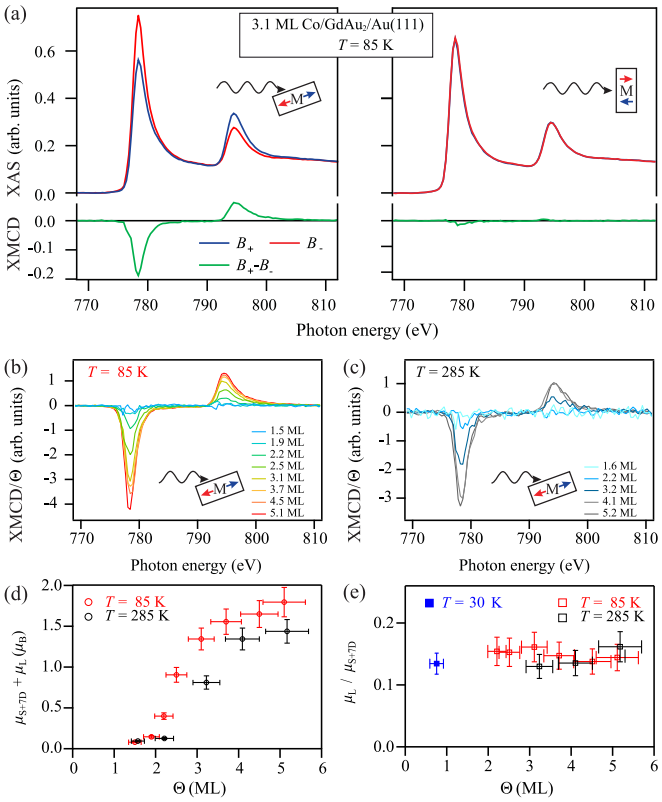

FIG. 4. (Color online) (a) Grazing ($\theta = 70°$) and normal ($\theta = 0°$) incidence XAS acquired with left circularly polarized x rays with the sample in remanence, once magnetized parallel and once antiparallel to the x rays after applying a field of 0.5 T as indicated in the sketches. The lower panels present the XMCD spectra. (b), (c) Remanent grazing incidence XMCD spectra for different coverages at $T = 85$ and 285 K, respectively. (d) Atomic magnetic moments $\mu_L + \mu_{S+7D}$ as a function of Θ at 85 and 285 K shown with red and black symbols, respectively. (e) μ_L/μ_{S+7D}, with the filled blue square indicating the $T = 30$ K value under an applied field of 6 T.

from inspection of the right-hand side of Fig. 4(a). Therefore the out-of-plane direction is a hard magnetization axis. This is quite remarkable, seeing that Co/Au(111) has an out-of-plane easy axis up to $\Theta = 4$ ML [20]. Alloying the Au surface with 1/3-ML Gd switches the easy axis of the adsorbed Co islands already for a thickness of two atomic layers, as seen above. This switching is maintained in the coalesced islands.

The emergence of in-plane remanence as a function of coverage is nicely seen from the coverage normalized grazing incidence XMCD spectra shown in Figs. 4(b) and 4(c) for $T =$ 85 and 285 K, respectively. At both temperatures, the remanent dichroic signal is negligible for $\Theta < 2.0$ ML, and it gradually increases for higher coverage. The threshold coverage for the onset of remanence is inferred from Fig. 4(d), where we show the total atomic moments $\mu_L + \mu_{S+7D}$ deduced from the remanent XMCD signal applying the sum rules [22,23]. The reported values take into account the degree of circular polarization of 80% and the photon incident angle of 70° assuming an in-plane easy axis. At $T = 85$ K the total atomic moments steeply rise between 2.0 and 3.0 ML until they saturate for $\Theta \geqslant 3.7$ ML at $(1.8 \pm 0.2)\mu_B$ per atom, quite close to the Co bulk value ($1.72\mu_B$) and slightly smaller than the Co monolayer value (2.1–$2.3\mu_B$ [34,35]). Data points interpolation identifies 2.2 ML as the onset of remanence at 85 K. At this coverage the clusters extend at least over three moiré cells and they cover an area of more than 1700 Å^2; see Fig. 1(g). Raising T to 285 K shifts the onset of remanence by 0.8 ML to $\Theta = 3.0$ ML. This is expected for systems where the exchange interaction is responsible for the long-range ferromagnetic order [36]. The ratio between remanent orbital and effective spin moments μ_L/μ_{S+7D} are shown in Fig. 4(e). They are situated at 0.13–0.16, thus comparing well to Co monolayers on Rh(111) with $\mu_L/\mu_{S+7D} = 0.16 \pm 0.04$, and on Pt(111) with 0.17 ± 0.04 [34,35].

Unlike expected for single element systems [37], no μ_L anisotropy variation is observed in our system, as testified by the almost constant μ_L/μ_{S+7D} ratio as a function of Θ, and thus as a function of cluster thickness and across the MAE reorientation transition; see Fig. 4(e). Thus, the effects of spin-orbit coupling on the entire hybridized system need to be considered to predict the magnetic anisotropy [38].

Magnetization curves acquired with MOKE provide additional information, first on the magnetization reversal process, and second they enable us to determine more precisely the coercive field H_c. The transverse MOKE $M(H)$ curves shown in Figs. 5(a) and 5(b) determine the onset of remanence at $T = 100$ K between 2.0 and 2.5 ML in excellent agreement with our XMCD data at 85 K. Out-of-plane polar MOKE $M(H)$ curves are fully reversible and exhibit a constant slope without any sign of saturation up to 0.3 T [39]. This confirms the out-of-plane hard axis. Note that the observed coercive fields, and therefore the related energy barriers, bear no connection with those of Co films on Au(111) that have an out-of-plane easy axis. The longitudinal MOKE $M(H)$ curves shown in Figs. 5(c) and 5(d) demonstrate that H_c is nearly coverage independent. As expected, it is slightly larger at lower temperature, $H_c(120\,\text{K}) = 4.3 \pm 0.3$ mT vs $H_c(300\,\text{K}) = 3.4 \pm 0.3$ mT.

According to the results presented in this paper, the previously published observation of room-temperature magnetic

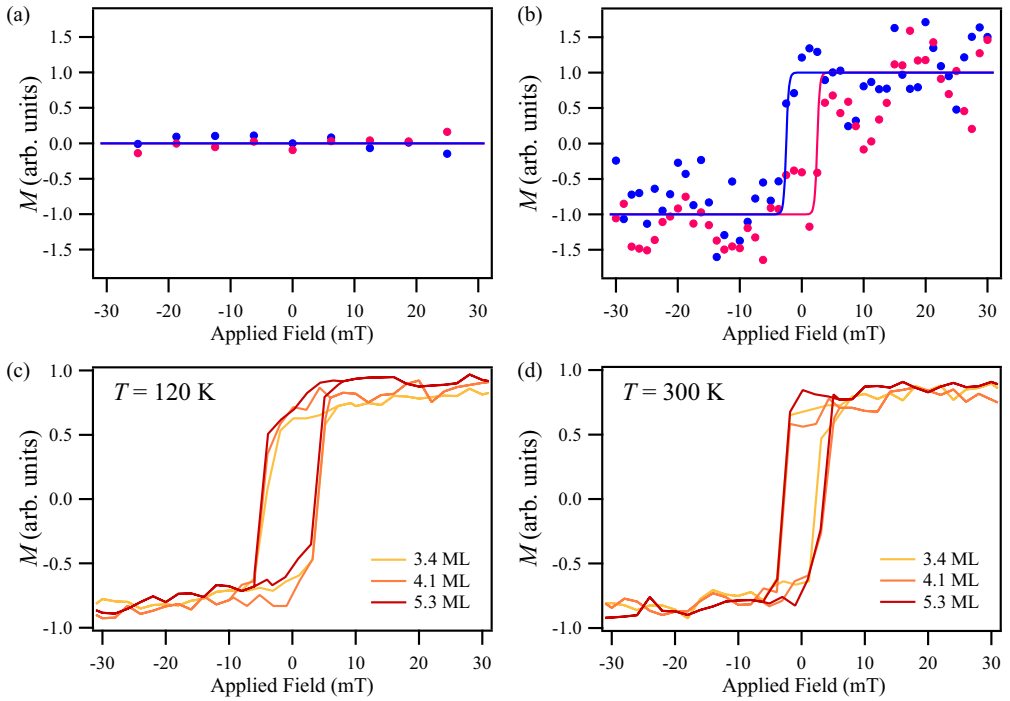

FIG. 5. (Color online) Transversal MOKE measurements at $T = 100$ K for (a) $\Theta = 2.0$ and (b) 2.5 ML. The magnetization curve measured while increasing (decreasing) the magnetic field is shown as purple (blue) symbols. Continuous lines are only intended as guides to the eye. (c),(d) Longitudinal MOKE for the coverages and temperatures indicated.

remanence for $Co/GdAu_2/Au(111)$ [4] can be rationalized considering that cluster coalescence may have taken place at the reported thickness of the spin-resolved photoemission experiment.

IV. CONCLUSIONS

We investigated the morphology-dependent magnetic properties of Co nanoclusters self-assembled on the $GdAu_2/Au(111)$-(13×13) template. We determine the morphological coalescence threshold of the Co islands at 1.5 ML. At smaller coverages we observe the coexistence of 1-AL-high islands with out-of-plane easy axis of magnetization axis and of 2–3-AL-high islands with in-plane easy axis. For the 1-AL islands we find a strong enhancement of the perpendicular magnetic anisotropy energy compared to a similar amount of Co on Au(111). For coverages above the coalescense threshold, nearly all islands are more than one atomic layer thick. They exhibit an in-plane easy axis. We find magnetic remanence at $\Theta = 2.2$ ML for $T = 85$ K, and at $\Theta = 3.0$ ML for room temperature. Above these values, the coercive fields detected by MOKE and the orbital moments observed by XMCD are temperature and coverage independent. This suggest long-range ferromagnetic order due to exchange interaction and filmlike magnetization reversal.

ACKNOWLEDGMENTS

The authors acknowledge the personnel of Circular Polarization and DEIMOS beamlines for technical support, and Elettra-Sincrotrone Trieste and Soleil for provision of synchrotron radiation. We acknowledge funding from the Swiss National Science Foundation, from the Sino-Swiss Science and Technology Cooperation Project No. IZLCZ2 123892, from the Spanish Ministerio de Ciencia e Innovación (MAT2010-21156-C03-03), from the Gipuzkoako Foru Aldundia, from the European Social Fund within the program JAE-Doc, the Basque Government (IT-621-13 and IT-627-13) and SAIOTEK (S-PE12UN095), as well as from the EU Calipso program for synchrotron access funding. The MBE chamber on DEIMOS was funded by the Agence National de la Recherche with Grant No. ANR-05-NANO-073.

[1] H. Brune, M. Giovannini, K. Bromann, and K. Kern, Nature (London) **394**, 451 (1998).
[2] M. Corso, M. J. Verstraete, F. Schiller, M. Ormaza, L. Fernández, T. Greber, M. Torrent, A. Rubio, and J. E. Ortega, Phys. Rev. Lett. **105**, 016101 (2010).
[3] M. Corso, L. Fernández, F. Schiller, and J. E. Ortega, ACS Nano **4**, 1603 (2010).
[4] L. Fernández, M. Corso, F. Schiller, M. Ilyn, M. Holder, and J. E. Ortega, Appl. Phys. Lett. **96**, 013107 (2010).
[5] N. Weiss, T. Cren, M. Epple, S. Rusponi, G. Baudot, S. Rohart, A. Tejeda, V. Repain, S. Rousset, P. Ohresser, F. Scheurer, P. Bencok, and H. Brune, Phys. Rev. Lett. **95**, 157204 (2005).

[6] C. Vo-Van, S. Schumacher, J. Coraux, V. Sessi, O. Fruchart, N. B. Brookes, P. Ohresser, and T. Michely, Appl. Phys. Lett. **99**, 142504 (2011).

[7] V. Sessi, S. Hertenberger, J. Zhang, D. Schmitz, S. Gsell, M. Schreck, R. Morel, A. Brenac, J. Honolka, and K. Kern, J. Appl. Phys. **113**, 123903 (2013).

[8] O. S. Anilturk and A. R. Koymen, Phys. Rev. B **68**, 024430 (2003).

[9] M. Colarieti-Tosti, M. I. Katsnelson, M. Mattesini, S. I. Simak, R. Ahuja, B. Johansson, C. Dallera, and O. Eriksson, Phys. Rev. Lett. **93**, 096403 (2004).

[10] M. Colarieti-Tosti, T. Burkert, O. Eriksson, L. Nordström, and M. S. S. Brooks, Phys. Rev. B **72**, 094423 (2005).

[11] S. Abdelouahed and M. Alouani, Phys. Rev. B **79**, 054406 (2009).

[12] Note that the Co coverage values in [2,4,28] are expressed in ML on $GdAu_2$ and do not coincide with those presented in this paper.

[13] A. Lehnert, P. Buluschek, N. Weiss, J. Giesecke, M. Treier, S. Rusponi, and H. Brune, Rev. Sci. Instrum. **80**, 023902 (2009).

[14] H. Brune, H. Röder, K. Bromann, and K. Kern, Thin Solid Films **264**, 230 (1995).

[15] C. Wöll, S. Chiang, R. J. Wilson, and P. H. Lippel, Phys. Rev. B **39**, 7988 (1989).

[16] J. V. Barth, H. Brune, G. Ertl, and R. J. Behm, Phys. Rev. B **42**, 9307 (1990).

[17] B. Voigtländer, G. Meyer, and N. M. Amer, Phys. Rev. B **44**, 10354 (1991).

[18] P. Ohresser, E. Otero, F. Choueikani, K. Chen, S. Stanescu, F. Deschamps, T. Moreno, F. Polack, B. Lagarde, J.-P. Daguerre, F. Marteau, F. Scheurer, L. Joly, J.-P. Kappler, B. Muller, O. Bunau, and Ph. Sainctavit, Rev. Sci. Instrum. **85**, 013106 (2014).

[19] A. Derossi, F. Lama, M. Piacentini, T. Prosperi, and N. Zema, Rev. Sci. Instrum. **66**, 1718 (1995).

[20] R. Allenspach, M. Stampanoni, and A. Bischof, Phys. Rev. Lett. **65**, 3344 (1990).

[21] S. Pütter, H. F. Ding, Y. T. Millev, H. P. Oepen, and J. Kirschner, Phys. Rev. B **64**, 092409 (2001).

[22] B. T. Thole, P. Carra, F. Sette, and G. van der Laan, Phys. Rev. Lett. **68**, 1943 (1992).

[23] P. Carra, B. T. Thole, M. Altarelli, and X. Wang, Phys. Rev. Lett. **70**, 694 (1993).

[24] C. T. Chen, Y. U. Idzerda, H.-J. Lin, N. V. Smith, G. Meigs, E. Chaban, G. H. Ho, E. Pellegrin, and F. Sette, Phys. Rev. Lett. **75**, 152 (1995).

[25] B. T. Thole, G. van der Laan, J. C. Fuggle, G. A. Sawatzky, R. C. Karnatak, and J.-M. Esteva, Phys. Rev. B **32**, 5107 (1985).

[26] A. Arrott, Phys. Rev. **108**, 1394 (1957).

[27] P. K. Manna and S. M. Yusuf, Phys. Rep. **535**, 61 (2014).

[28] L. Fernández, M. Blanco-Rey, M. Ilyn, L. Vitali, A. Magaña, A. Correa, P. Ohresser, J. E. Ortega, A. Ayuela, and F. Schiller, Nano Lett. **14**, 2977 (2014).

[29] S. Rohart, V. Repain, A. Tejeda, P. Ohresser, F. Scheurer, P. Bencok, J. Ferré, and S. Rousset, Phys. Rev. B **73**, 165412 (2006).

[30] P. Gambardella, S. Rusponi, M. Veronese, S. S. Dhesi, C. Grazioli, A. Dallmeyer, I. Cabria, R. Zeller, P. H. Dederichs, K. Kern, C. Carbone, and H. Brune, Science **300**, 1130 (2003).

[31] Both size distributions satisfy the condition that the average cluster size is $13 \times 13 \times 0.75 = 127$ atoms, corresponding to the coverage of 0.75 ML on the (13×13) moiré unit cell.

[32] T. Koide, H. Miyauchi, J. Okamoto, T. Shidara, A. Fujimori, H. Fukutani, K. Amemiya, H. Takeshita, S. Yuasa, T. Katayama, and Y. Suzuki, Phys. Rev. Lett. **87**, 257201 (2001).

[33] S. Rohart, P. Campiglio, V. Repain, Y. Nahas, C. Chacon, Y. Girard, J. Lagoute, A. Thiaville, and S. Rousset, Phys. Rev. Lett. **104**, 137202 (2010).

[34] G. Moulas, A. Lehnert, S. Rusponi, J. Zabloudil, C. Etz, S. Ouazi, M. Etzkorn, P. Bencok, P. Gambardella, P. Weinberger, and H. Brune, Phys. Rev. B **78**, 214424 (2008).

[35] A. Lehnert, S. Dennler, P. Błoński, S. Rusponi, M. Etzkorn, G. Moulas, P. Bencok, P. Gambardella, H. Brune, and J. Hafner, Phys. Rev. B **82**, 094409 (2010).

[36] R. Brinzanik, P. J. Jensen, and K. H. Bennemann, Phys. Rev. B **68**, 174414 (2003).

[37] P. Bruno, Phys. Rev. B **39**, 865 (1989).

[38] C. Andersson, B. Sanyal, O. Eriksson, L. Nordström, O. Karis, D. Arvanitis, T. Konishi, E. Holub-Krappe, and J. Hunter Dunn, Phys. Rev. Lett. **99**, 177207 (2007).

[39] A. Cavallin, Ph.D. thesis, École Polytechnique Fédérale de Lausanne, 2013.